Chapter 3
Three-Dimensional Flight Simulation with Transient Moving-Aerofoil Models

Arion Pons and Fehmi Cirak

Abstract The simulation of highly transient three-dimensional flight has relevance to several areas of current aerospace research, including the design of biomimetic micro-air vehicles. Modelling transient aerofoil motion in such systems is difficult due to the competing demands of model fidelity and computation time. In this work we present a fully three-dimensional flight simulator for biomimetic moving-wing aircraft, using a Goman-Khrabrov type model to capture transient aerodynamic effects. Parameters for this model are identified from quasistatic data and transient computational fluid dynamics, with a quantitative assessment of the model's limitations. Flight simulation results are presented for a Pugachev cobra manoeuvre, and the significance of transient aerodynamic modelling is demonstrated.

Keywords Biomimetic · Flight simulation · Aerodynamics · Goman-Khrabrov

3.1 Flight Simulator Framework

3.1.1 Biomimetic Systems

Biomimetic flapping aircraft have seen significant study over a wide range of scales: biomimetic insects [1, 2], pigeons [3], bats [4, 5], and pterosaurs [6, 7] have been considered, among many others. A key impediment to their practical implementation—particularly in high-performance applications—is the difficulty of flight modelling and analysis, arising from the complexity of flapping-wing aerodynamics. High-fidelity computational models are often required [8, 9], which limits the scope of analysis that may be carried out.

In this work we devise reduced-order models for the transient post-stall aerodynamic analysis of a flapping wing system, with a target scale of c. 1 m (e.g. larger biomimetic vertebrates), and a characteristic wing Reynolds number of c. 3×10^5.

A. Pons (✉) · F. Cirak
University of Cambridge, Cambridge CB2 1PZ, UK
e-mail: adp53@cam.ac.uk

S. Gutschmidt et al. (eds.), *IUTAM Symposium on Recent Advances in Moving Boundary Problems in Mechanics*, IUTAM Bookseries 34,
https://doi.org/10.1007/978-3-030-13720-5_3

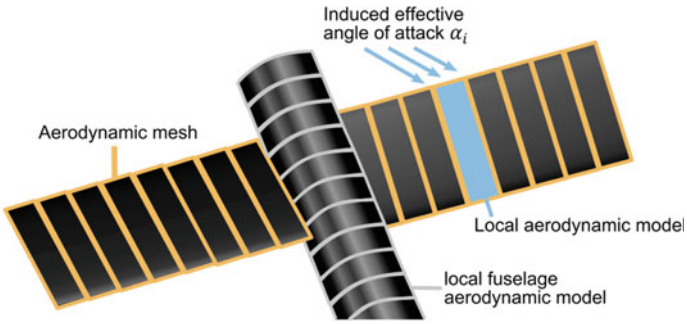

Fig. 3.1 Schematic of aerodynamic mesh framework

This is implemented in a flight simulator for a hybrid biomimetic aircraft; consisting of a conventional propulsion system (e.g. propeller) coupled with three degree-of-freedom wing rotation to enable biomimetic supermanoeuvrability—highly transient, post-stall manoeuvres. The inclusion of transient post-stall aerodynamic effects is self-evidently a key factor in accurately simulating such manoeuvres.

3.1.2 Structural Dynamics and Integration

Multibody dynamics are used to describe the structural behaviour of the modelled aircraft. All system internal degrees of freedom (e.g. wing motion) are assumed to be actuated, leading to a six degree-of-freedom system model which nevertheless includes the inertial effects of wing motion exactly. The system orientation is parameterized with an orientation quaternion, and the system model is integrated with a quaternion variational integrator, similar to that of Manchester and Peck [10].

3.1.3 Aerodynamic Framework

The system aerodynamics are formulated in a strip theory/blade element momentum framework. Each component of the airframe, lifting surface or otherwise, is discretized along its major axis into a series of two-dimensional section models. Local aerodynamic quantities at each section model are computed from the body kinematics (including the effect of wing motion-induced flow) and resolved into polar coordinates, leading to local values of the effective angle of attack α_i, its rate $\dot{\alpha}_i$, and the airspeed U. Figure 3.1 shows a schematic of this discretization process.

This framework neglects the effects of spanwise flow and of flow shadowing or other interactions within the airframe. While the aerodynamic mesh framework does

not preclude the modelling of spanwise flow or inter-section coupling effects, no models to this end have yet been suggested in the literature.

The aerofoil considered in this paper is the wing aerofoil (ST50W) from the ShowTime 50, an existing highly-manoeuvrable remote-control aircraft. This aerofoil is used for the wings of the case study biomimetic system. Quasistatic data for this aerofoil is available from Selig [11]. The stabilisers use other aerofoils, which contain control surfaces. The modelling approach for these aerofoils is not covered in this paper.

3.2 Goman-Khrabrov (GK) Modelling

3.2.1 Transient Aerodynamic Models

In situations where computational models of transient aerodynamic effects are unfeasible, some form of lower-order dynamic stall and lift hysteresis model is required. Phenomenological models of this form include the ONERA [12] and Goman-Khrabrov (GK) [13] models, among others [14]. Model reduction techniques are also available [15–17], though these still require higher-fidelity data to work on. At a simpler level, Theodorsen's aerodynamic theory provides a method by which the dynamic effects of low-amplitude pitching and dihedral motion may be modelled [18, 19]; though the method does not extend to large amplitudes [20]. Wagner's indicial response function [20] and the finite-state theory of Peters et al. [21] perform similar roles. Few of these methods, however, have been applied to morphing-wing systems.

In this work we apply a GK model to our biomimetic system. The application of such a model to fully three-dimensional flight simulation requires some significant extensions and generalisations. Here the phenomenological nature of this model is a significant advantage, as physical reasoning can be utilised to diagnose the causes of model breakdown, and to guide the model identification process.

3.2.2 GK Model Formulation

The Goman-Khrabrov dynamic stall model may be expressed as follows. For any section model, the aerodynamic coefficients (lift, drag and moment) are decomposed into attached-flow $\left(C_{i,\mathrm{att}}\right)$ and separated-flow $\left(C_{i,\mathrm{sep}}\right)$ components, each as a function of angle of attack α. These components are then recomposed with a mixing parameter p, describing the degree of local flow separation:

$$C_i(\alpha) = pC_{i,\mathrm{att}}(\alpha) + (1-p)C_{i,\mathrm{sep}}(\alpha). \tag{3.1}$$

In a fully attached flow regime $p = 0$, and in a fully separated flow regime $p = 1$; and thus the behaviour of p only governs the system aerodynamic behaviour in the transition zone. In Goman and Khrabrov's original model [13], p was related directly to the location of the flow separation point along the airfoil chord; $p = 1$ representing separation at the leading edge and $p = 0$ at the trailing edge, i.e. not at all. However, more modern approaches [22–24] have loosened this direct relation in favour of a parameter-identification approach.

In the case of aerofoil quasistatic motion, the behaviour of p is governed solely by a quasistatic mixing function, $p = p_0(\alpha)$, representing the flow separation progression through the transition region. Note that it is possible to account for static lift hysteresis here, by defining separate p_0^+ and p_0^- functions representing quasistatic pitch-up and pitch-down motion [22]; but we do not consider this here. In the case of transient motion, p is modelled by a first-order ordinary differential equation:

$$\tau_1 \dot{p} = p_0(\alpha - \tau_2 \dot{\alpha}), \tag{3.2}$$

where $\{\tau_1, \tau_2\}$ are delay times, corresponding respectively to the system time constant (i.e. the system delay in responding to a change in state) and the separation-delaying effect of pitch rate ($\dot{\alpha}$). With an accurate identification of the delays $\{\tau_1, \tau_2\}$, quasistatic mixing function $p_0(\alpha)$ and separated and attached flow models $C_{i,\text{att}}$ and $C_{i,\text{sep}}$, accurate models of transient airfoil pitching model may be obtained [22].

3.2.3 *Identification of Quasistatic Model Parameters*

A key distinction may be made in the GK model between quasistatic and dynamic model parameters. The former, $p_0(\alpha)$, $C_{i,\text{att}}(\alpha)$ and $C_{i,\text{sep}}(\alpha)$, are features of the decomposition of aerodynamic coefficients into separated and attached components, and are thus not directly associated with any dynamic effects. They may be identified directly from quasistatic data. The attached flow regime is modelled well by linear relations, as per potential flow theory, whereas the separated flow regime is modelled well by sinusoids, as per separated-flow thin-aerofoil theory [23]. We in fact propose a split sinusoid model, as this yields a significantly better fit; particularly for the drag and moment coefficients:

$$\begin{aligned} C_{i,\text{sep}}(\alpha) &= A_i \sin(B_i|\alpha - C_i| + D_i), \\ C_{i,\text{att}}(\alpha) &= \begin{cases} E_i\alpha + F_i & -90^\circ \leq \alpha \leq 90^\circ \\ G_i(\alpha - 180^\circ) + H_i & 90^\circ < \alpha \leq 180^\circ \\ G_i(\alpha + 180^\circ) + H_i & -180^\circ \leq \alpha < -90^\circ, \end{cases} \end{aligned} \tag{3.3}$$

with coefficients $A_i - H_i$. It should be noted that, in a fully three-dimensional flight simulator, cases of lifting surface reverse flow ($\alpha \cong 180^\circ$) may occur. An identification of trailing edge $p_0(\alpha)$ and $C_{i,\text{att}}(\alpha)$ are thus also required: hence the

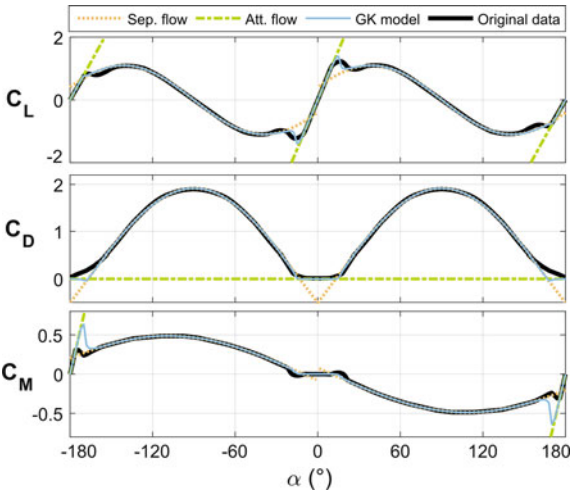

Fig. 3.2 Aerodynamic coefficients for the ST50W: attached and separated flow models, original data, and reconstructed model

formulation $C_{i,\mathrm{att}}(\alpha)$, which additionally accounts for the discontinuity (between $\pm 180°$) at this location. Phenomenologically the leading and trailing edge models are unlikely to be identical on account of the sharp tip on the trailing edge—leading to more rapid flow separation and a change in the attached flow gradients. The identification and implementation of a full leading and trailing edge GK model has not been attempted before.

A direct identification of p_0 is more difficult, and typically requires a large number of data points within the transitional flow regime (c.f. [22]). When this is not available, and particularly when considering multiple aerodynamic coefficients (lift, drag and moment) direct identification is not possible. To overcome this, Reich et al. [23] proposed a general empirical result, an inverse tangent sigmoid. Applied to the leading and trailing edge the model may be expressed:

$$p_0(\alpha) = \begin{cases} -0.0058\,\tan^{-1}(w_+|\alpha| + 16) + 0.5 & -90^\circ \le \alpha \le 90^\circ \\ -0.0058\,\tan^{-1}(w_-(|\alpha| - 180) + 16) + 0.5 & 90^\circ < |\alpha| \le 180^\circ. \end{cases} \tag{3.4}$$

As an addition, we include a width parameter $w_\pm$ ($= 1$ in Reich et al. [23]) for the purpose of modelling the aerofoil trailing edge.

The quasistatic model specification is now complete. Figure 3.2 shows the attached and separated flow models identified from the quasistatic ST50W data of Selig [11]. Figure 3.3 shows the empirical p_0 model from Reich et al. [23], compared with the results of results generated by a direct identification, which may be obtained simply by solving Eq. 3.1 for p at each quasistatic data point. The trailing edge results are presented around $\alpha = 0$ for convenience. Figure 3.2 shows additionally the GK reconstruction of the quasistatic data, computed with $p = p_0(\alpha)$ in Eq. 3.1.

As can be seen, the identification of the separated and attached flow models is very good: the split sinusoid model performs significantly better than a plain sinusoid

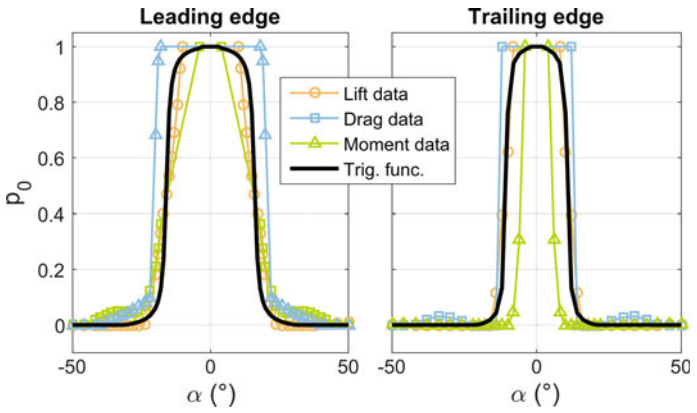

Fig. 3.3 Identified $p_0(\alpha)$ functions for the ST50W, compared with the arctangent sigmoid

would, as can be noted by the significant non-zero values of the separated flow models at $\alpha = 0$. The empirical result for p_0 also represents a good fit: for the leading edge we have $w_+ = 1$ as per Reich et al. [23]; for the trailing edge $w_- = 1.6$ to match the profile observed in the lift and drag coefficient data. There is a degree of spread in the directly identified p_0 profiles, notably in the trailing edge moment coefficient, and this leads to a degree of error in the reconstructed quasistatic profiles (again, notably in the trailing edge moment coefficient). However, attempting to extend the model to a unique $p_0(\alpha)$ function in each coefficient breaks the physical relevance of p and yields a model which ceases to have any phenomenological basis. Overall, a single $p_0(\alpha)$ is adequate. This completes the identification of the quasistatic parameters.

3.2.4 Identification of Transient Model Parameters

To identify the dynamic delay times $\{\tau_1, \tau_2\}$ we turn to computational fluid dynamics (CFD). A two-dimensional transient flow simulation of the aerofoil at Reynolds number 3×10^5 is created in OpenFoam, equipped with a moving-mesh solver to allow arbitrary specified in-plane wing motion. Figure 3.4 shows the simulation geometry, along with the standard simulation mesh and the velocity and pressure boundary conditions. Turbulence in the flow domain is modelled using the Menter shear-stress-transport model [25] with wall functions to resolve the boundary layer. The turbulent kinetic energy and specific rate of dissipation boundary conditions are all switching conditions which take a fixed freestream value on cells with flow into the domain, and constrained to zero gradient on cells with outward flow.

The flow initial conditions are supplied via a steady state solution to system at the initial aerofoil orientation, obtained via the SIMPLE algorithm [26]. The transient flow equations are solved using the PIMPLE algorithm, an OpenFoam-

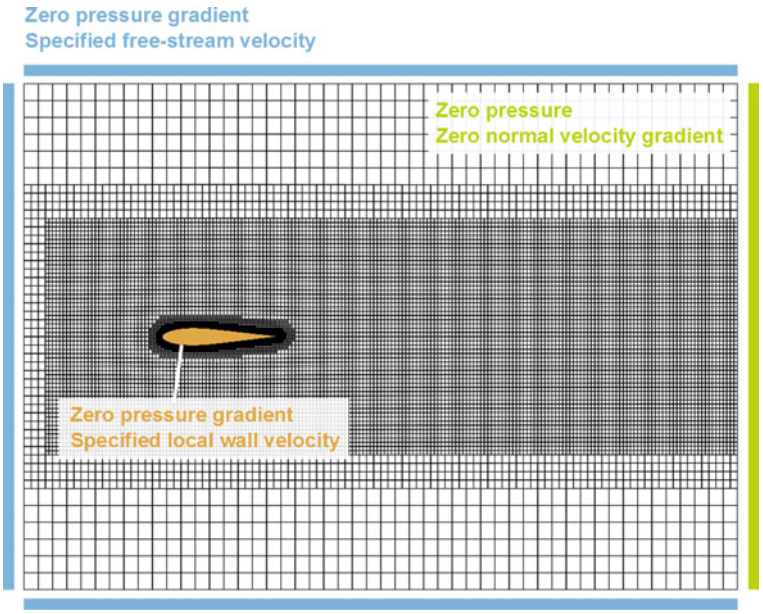

Fig. 3.4 Schematic of CFD model geometry and mesh, with boundary conditions

specific combination of the SIMPLE and PISO algorithms [27]. A mesh convergence analysis is carried out. Aerodynamic coefficient results for simulations at fixed angle-of-attack are notably larger than those reported in Selig [11], as a result of closed-jet tunnel conditions (c.f. [28]) generated by the moderately-sized domain size. However, as the identification of $\{\tau_1, \tau_2\}$ is independent of the magnitude of the aerodynamic components, this is not a fundamental difficulty: the quasistatic model parameters can be re-identified for the closed-jet tunnel results. Then, under the assumption that the closed-jet conditions do not fundamentally alter the nature or timescale of the dynamic stall event, the identified $\{\tau_1, \tau_2\}$ may be applied to the original model. While a larger domain size could remove this need for re-identification, the smaller closed-jet tunnel domain allows a larger number of simulations to be carried out for an equivalent computational effort.

Results from the simulation of sinusoidal pitching motion at several reduced frequencies are used to identify $\{\tau_1, \tau_2\}$. These reduced frequencies are defined as $k = b\omega/U$, where b is the aerofoil semichord, U the airspeed and ω the dimensional oscillatory frequency. A reasonable match for reduced frequencies below $k = 0.70$ is found to be $\tau_1 = 1b/U$, $\tau_2 = 3b/U$. Figures 3.5, 3.6 and 3.7 shows the GK model predictions compared with the CFD data for results at $k = 0.175, 0.35, 0.70$ (0.5, 1.0 and 2.0 Hz). The quasistatic coefficient curve, in the absence of GK modelling, is also noted. As can be seen, a reasonable quantitative match is obtained. The observed noise effects (e.g. Fig. 3.6) are related to the transition between attached and separated flow regimes. A notable result is that of $k = 0.70$: the CFD dynamic

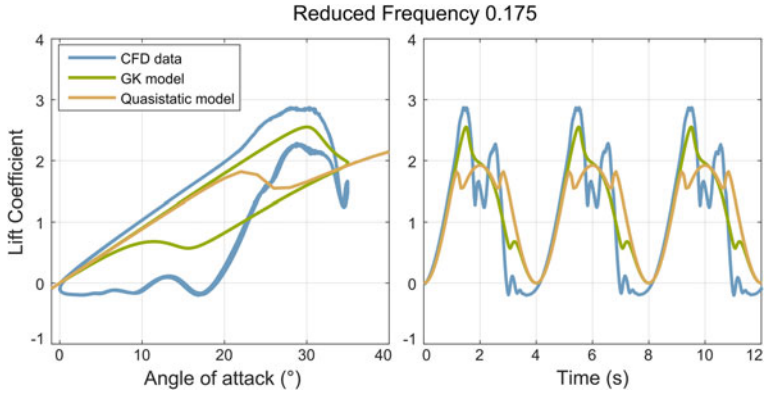

Fig. 3.5 GK model and CFD lift coefficient results for $k = 0.175$

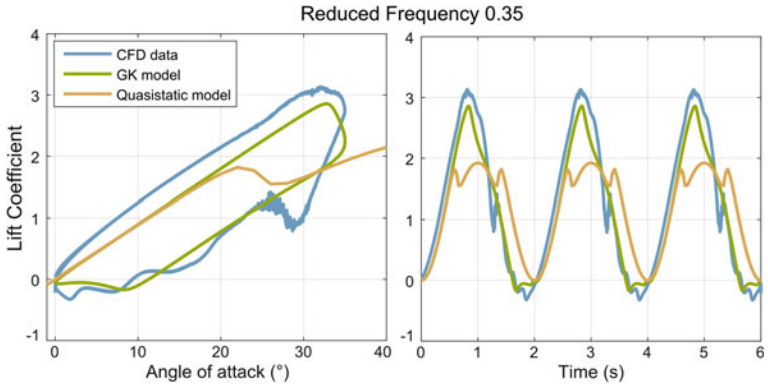

Fig. 3.6 GK model and CFD lift coefficient results for $k = 0.35$

stall loop in angle-of-attack space is of similar size and shape, but at significantly higher coefficient values. This difference is attributable to added mass effects, and indicates the beginning of model breakdown.

3.2.5 Limitations on the Identification of Transient Parameters

Severe model breakdown is observed above $k = 1.40$ (2 Hz): Fig. 3.8 demonstrates this effect. The broad elliptical coefficient curves are characteristic of added mass effects, as in Theodorsen's aerodynamic theory [29]. However, it is not clear how such models of added mass effects can be synthesised with the GK model, especially as the former are typically expressed in the frequency domain [29]. Until such synthesis

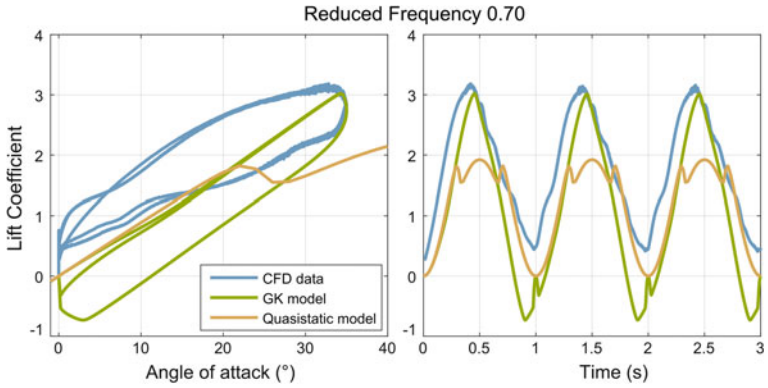

Fig. 3.7 GK model and CFD lift coefficient results for $k = 0.70$

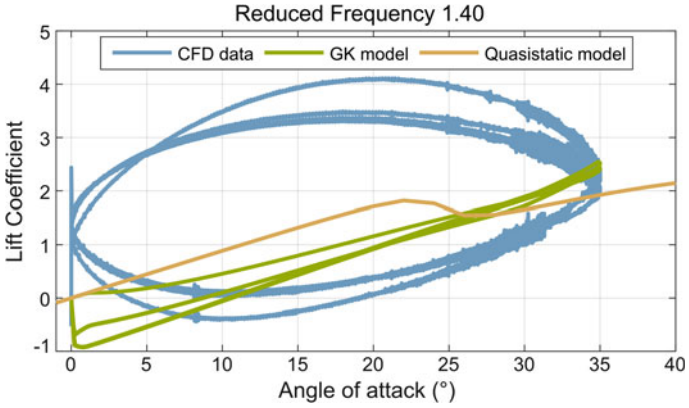

Fig. 3.8 GK model and CFD lift coefficient results for $k = 1.40$

models are developed, this aerodynamic model must be regarded as valid only up to $k = 0.70$.

3.3 Flight Simulation

3.3.1 Cobra Manoeuvre

As a test case, we simulate a Pugachev cobra manoeuvre [30] carried out by a biomimetic morphing-wing system. The manoeuvre is designed via longitudinal stability analysis: this process is not presented here. Figure 3.9 however shows the manoeuvre, simulated with GK and quasistatic aerodynamic models. As can be seen,

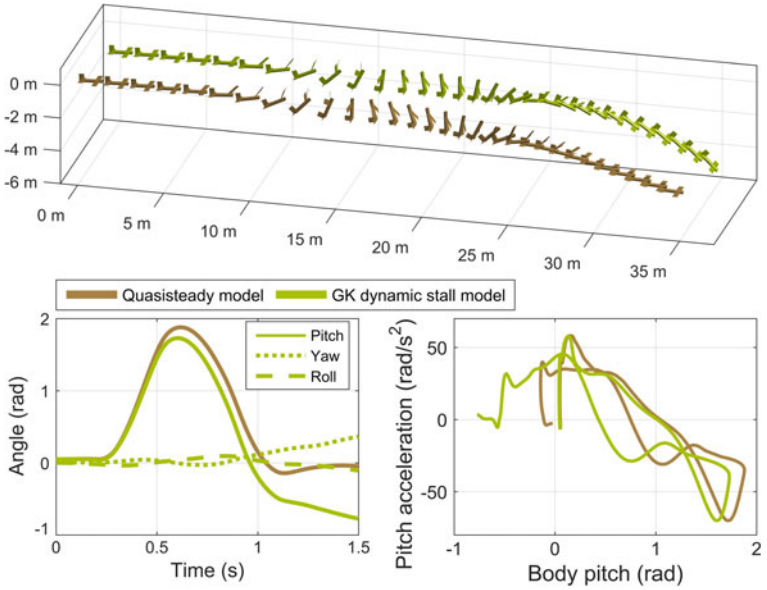

Fig. 3.9 Flight simulation results for the Pugachev cobra manoeuvre, for GK and quasistatic aerodynamic models

the implementation of GK modelling has a significant effect on the manoeuvre: delayed reattachment in the later phases of the manoeuvre leads to a much longer duration of pitch-down moment, drawing the aircraft into a dive. Changes of control design are thus required to avoid this effect—demonstrating the relevance of GK modelling to this system.

3.3.2 Spectral Analysis

To check whether the Pugachev cobra manoeuvre breaches the validity conditions of the GK model, we perform a spectral analysis of the angle-of-attack history of the GK simulation. Under the Fourier transform, $\alpha(t) = \hat{\alpha}\exp(i\omega t)$, the system spectrum in ω may be used to estimate the spectrum in reduced frequency; $k = b\omega/U$. We base this estimate on the (left) wingtip angle of attack: the location showing the greatest induced flow from wing motion. However, as U is a time-domain quantity, we compute $\max(k)$ and $\min(k)$ over the manoeuvre history based on the maximum and minimum U. Figure 3.10 shows the time-domain history of the wingtip α and its corresponding reduced-frequency spectrum, with the GK model validity boundary at $k = 0.70$ noted. As can be seen, even under the most conservative estimate, the manoeuvre contains negligible frequency components above the model validity boundary. This analysis demonstrates the validity of this Pugachev cobra

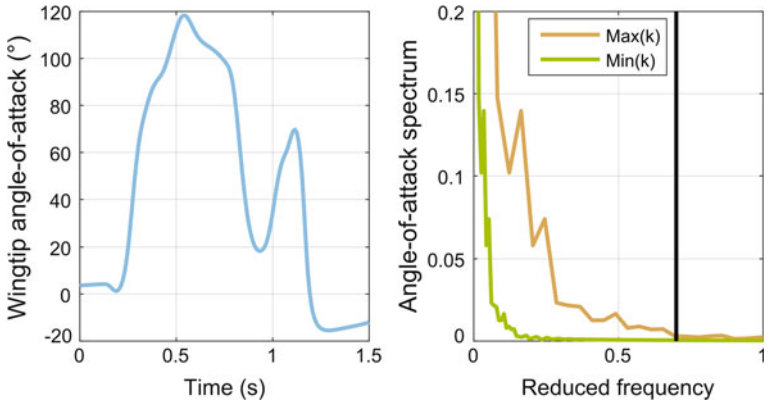

Fig. 3.10 Time-domain history and reduced frequency spectrum of the left wingtip angle-of-attack during the Pugachev cobra manoeuvre (GK model simulation)

simulation with the GK model, and provides a method of assessing the validity of these frequency-dependent aerodynamic models applied to other strongly transient flight simulations. This confirms the noted significance of the GK model to the control and guidance of this supermanoeuvre, as carried out by the biomimetic morphing-wing system considered in this work.

3.4 Conclusion

In this work we have presented a fully three-dimensional flight simulator for biomimetic moving-wing aircraft, including a Goman-Khrabrov (GK) type model to capture transient aerodynamic effects. We identify parameters for the GK model from quasistatic data and simulations of the transient aerodynamics via computational fluid dynamics, and we give a quantitative assessment of the model's limitations. Flight simulation results are presented for a Pugachev cobra manoeuvre, demonstrating both the potential of biomimetic systems for complex post-stall manoeuvring, and the significance of transient aerodynamic modelling for such manoeuvres. For future work, there is scope for the development of more accurate models based on larger computational fluid dynamic data sets, and including added mass and Reynolds number effects. There is also the potential for the design and simulation of more complex post-stall manoeuvres in biomimetic systems; and for applications in high-performance biomimetic unmanned aerial vehicles.

References

1. Graule, M.A., Chirarattananon, P., Fuller, S.B., Jafferis, N.T., Ma, K.Y., Spenko, M., Kornbluh, R., Wood, R.J.: Perching and takeoff of a robotic insect on overhangs using switchable electrostatic adhesion. Science **352**(6288), 978–982 (2016)
2. Ma, K.Y., Chirarattananon, P., Fuller, S.B., Wood, R.J.: Controlled flight of a biologically inspired, insect-scale robot. Science **340**(6132), 603–607 (2013)
3. Mahardika, N., Nguyen, Q.V., Park, H.C.: A pigeon-inspired design for a biomimetic flapping wing. In: Ghasemi-Nejhad, M.N. (ed.) Active and Passive Smart Structures and Integrated Systems 2010, SPIE, pp. 76431Q-76431Q–11. SPIE, Bellingham, WA (2010)
4. Furst, S.J., Bunget, G., Seelecke, S.: Design and fabrication of a bat-inspired flapping-flight platform using shape memory alloy muscles and joints. Smart Mater. Struct. **22**(1), 014011 (2013)
5. Recchiuto, C.T., Molfino, R., Hedenströem, A., Peremans, H., Cipolla, V., Frediani, A., Rizzo, E., Muscolo, G.G.: Bioinspired mechanisms and sensorimotor schemes for flying: a preliminary study for a robotic bat. In: Mistry, M., Leonardis, A., Witkowski, M., Melhuish, C. (eds.) Advances in Autonomous Robotics Systems, pp. 37–47. Springer, Cham, Switzerland (2014)
6. Zakaria, M.Y., Taha, H.E., Hajj, M.R.: Design optimization of flapping ornithopters: the pterosaur replica in forward flight. J. Aircr. **53**(1), 48–59 (2015)
7. Roberts, B., Lind, R., Chatterjee, S.: Flight dynamics of a pterosaur-inspired aircraft utilizing a variable-placement vertical tail. Bioinspiration Biomim. **6**(2), 026010 (2011)
8. Culbreth, M., Allaneau, Y., Jameson, A.: High-fidelity optimization of flapping airfoils and wings. In: 29th AIAA Applied Aerodynamics Conference, AIAA, Honolulu, HI (2011)
9. Tuncer, I.H., Platzer, M.F.: Computational study of flapping airfoil aerodynamics. J. Aircr. **37**(3), 514–520 (2000)
10. Manchester, Z.R., Peck, M.A.: Quaternion variational integrators for spacecraft dynamics. J. Guid. Control Dyn. **39**(1), 69–76 (2016)
11. Selig, M.: Modeling Full-envelope aerodynamics of small UAVs in realtime. In: AIAA Atmospheric Flight Mechanics Conference, AIAA, Toronto, ON (2010)
12. McAlister, K.W., Lambert, O., Petot, D.: Application of the ONERA Model of Dynamic Stall. Technical Paper 2399, NASA, Washington, D.C. (1984)
13. Goman, M., Khrabrov, A.: State-space representation of aerodynamic characteristics of an aircraft at high angles of attack. J. Aircr. **31**(5), 1109–1115 (1994)
14. Holierhoek, J.G., de Vaal, J.B., van Zuijlen, A.H., Bijl, H.: Comparing different dynamic stall models: comparing different dynamic stall models. Wind Energy **16**(1), 139–158 (2013)
15. Brunton, S., Rowley, C.: Unsteady aerodynamic models for agile flight at low Reynolds number. In: 48th AIAA Aerospace Sciences Meeting, AIAA, Orlando, FL (2010)
16. Balajewicz, M., Nitzsche, F., Feszty, D.: Application of multi-input Volterra theory to nonlinear multi-degree-of-freedom aerodynamic systems. AIAA J. **48**(1), 56–62 (2010)
17. Wang, Q., Qian, W., He, K.: Unsteady aerodynamic modeling at high angles of attack using support vector machines. Chin. J. Aeronaut. **28**(3), 659–668 (2015)
18. Liska, S., Dowell, E.H.: Continuum aeroelastic model for a folding-wing configuration. AIAA J. **47**(10), 2350–2358 (2009)
19. Wang, I.: Aeroelastic and Flight Dynamics Analysis of Folding Wing Systems. Doctoral Dissertation, Duke University (2013)
20. Brunton, S., Rowley, C.: Modeling the unsteady aerodynamic forces on small-scale wings. In: 47th AIAA Aerospace Sciences Meeting, AIAA, Orlando, FL (2009)
21. Peters, D.A., Karunamoorthy, S., Cao, W.-M.: Finite state induced flow models. I—two-dimensional thin airfoil. J. Aircr. **32**(2), 313–322 (1995)
22. Williams, D.R., Reißner, F., Greenblatt, D., Müller-Vahl, H., Strangfeld, C.: Modeling lift hysteresis on pitching airfoils with a modified Goman-Khrabrov model. AIAA J. **55**(2), 403–409 (2017)
23. Reich, G.W., Eastep, F.E., Altman, A., Albertani, R.: Transient poststall aerodynamic modeling for extreme maneuvers in micro air vehicles. J. Aircr. **48**(2), 403–411 (2011)

24. Williams, D.R., An, X., Iliev, S., King, R., Reißner, F.: Dynamic hysteresis control of lift on a pitching wing. Exp. Fluids **56**(112) (2015)
25. Menter, F.R.: Two-equation Eddy-viscosity turbulence models for engineering applications. AIAA J. **32**(8), 1598–1605 (1994)
26. Ferziger, J.H., Perić, M.: Computational Methods for Fluid Dynamics. Springer, New York (2002)
27. Robertson, E., Choudhury, V., Bhushan, S., Walters, D.K.: Validation of OpenFOAM numerical methods and turbulence models for incompressible bluff body flows. Comput. Fluids **123**, 122–145 (2015)
28. Du, L., Berson, A., Dominy, R.G.: Aerofoil behaviour at high angles of attack and at Reynolds numbers appropriate for small wind turbines. Proc. Inst. Mech. Eng. Part C: J. Mech. Eng. Sci. **229**(11), 2007–2022 (2015)
29. Bisplinghoff, R.L., Ashley, H., Halfman, R.L.: Aeroelasticity. Addison-Wesley, Reading, MA (1957)
30. Ericsson, L.E.: Cobra maneuver unsteady aerodynamic considerations. J. Aircr. **32**(1), 214–216 (1995)